Early warning of drillstring faulty conditions based on multi-model fusion in geological drilling processes

Yupeng Li[a,b,c,d], Weihua Cao[a,b,c,*], R. Bhushan Gopaluni[d], Wenkai Hu[a,b,c], Min Wu[a,b,c]

[a]*School of Automation, China University of Geosciences, Wuhan 430074, China*
[b]*Hubei key Laboratory of Advanced Control and Intelligent Automation for Complex Systems, Wuhan 430074, China*
[c]*Engineering Research Center of Intelligent Technology for Geo-Exploration, Ministry of Education, Wuhan 430074, China*
[d]*Department of Chemical and Biological Engineering, University of British Columbia, Vancouver, BC V6T 1Z3, Canada*

Abstract

The early warning of drilling faults is of paramount importance to prevent or reduce environmental and property damages. In view of the complex drillstring kinematic characteristics and changeable formation environment, this paper proposes a new fault early warning method for the drillstring system based on a multi-model fusion and self-updating strategy. The major contributions are twofold: 1) A hybrid drillstring early warning method is proposed to identify faulty conditions based on the fusion of multi-dimensional prediction models of the drillstring system; 2) An event-triggered model self-updating strategy is proposed to mitigate the prediction performance degradation caused by formation uncertainties. The effectiveness and practicability of the proposed method are demonstrated by industrial case studies, and the results indicate that the proposed method outperforms other approaches.

Keywords: Drilling process, fault early warning, multi-model fusion, Wasserstein distance,

1. Introduction

Geological drilling is an indispensable process for deep geothermal development, geological prospecting, and mineral exploration. The complex geological environments with high temperature, high pressure, and high terrestrial stress contribute to undesirable drilling faults, such as drillstring failures, which can compromise human safety and increase the asset cost [1, 2]. Therefore, ensuring process safety has long been desired for geological drilling processes. In drilling processes, identifying the dynamically changing formation environment and processing multi-source heterogeneous data are challenging for a drilling operator, making downhole faults difficult to detect or predict timely [3, 4]. Therefore, a well-designed early warning system is paramount to prevent or reduce environmental and property damage caused by faults. The research topic on detecting downhole faults is commonly encountered in oil, natural gas, and geological drilling processes.

With the advent of modern information systems, data-driven methods have been extensively studied due to the availability of a large amount of process data [5, 6, 7]. Neural networks often provide superior performance in fitting the strong nonlinear relationship between drilling data and the corresponding faults [8, 9]. A 3D-convolutional neural network was used to detect early signs of a stuck pipe [10]. Fault diagnosis models were established using neural networks and Bayesian classifiers based on change features of drilling signals, such as multi-scale trend features and local trend features [11, 12]. Since obtaining data in faulty conditions is rather tricky in geological drilling, unsupervised learning methods were applied where almost no faulty data were available. An abnormality detection method was proposed based on clustering drilling conditions and establishing normal operating zones [13]. A prediction model for the stuck pipe fault is built based on the trend of the key signal captured using change point detection and moving-window regression [14]. Further, the dissimilarity between distributions is utilized to detect incipient downhole faults [15]. However, the data-driven fault diagnosis approach lacks mechanistic knowledge and primarily dependents on historical data, which can hardly cover all drilling conditions, and thus is prone to generate false alarms.

Recently, mechanical models were combined with data-driven methods to improve the robustness of the fault diagnosis method [16]. These methods effectively reflect the dynamic characteristics and variable dependencies in the drilling process. For instance, drilling incident diagnosis methods for the lost circulation and gas influx were proposed using mechanistic model-based adaptive observers and statistical change detection algorithms [17]. For the drillstring washout fault detection, a hydrodynamical model-based unscented Kalman filter was combined with a likelihood ratio test [18]. However, the previously men-

*Corresponding author at: School of Automation, China University of Geosciences, Wuhan 430074, China.
Email addresses: yupengli@cug.edu.cn (Yupeng Li), weihuacao@cug.edu.cn (Weihua Cao), bhushan.gopaluni@ubc.ca (R. Bhushan Gopaluni), wenkaihu@cug.edu.cn (Wenkai Hu), wumin@cug.edu.cn (Min Wu)

tioned approaches fall short in drillstring safety monitoring because they are designed based on the hydrodynamical model of the drilling fluid system, which is quite challenging to reflect the movements of the drillstring.

The development of the drillstring motion model has received increasing studies in the fields of stick-slip vibrations control and weight on bit control [19, 20]. A physically consistent nonlinear drillstring model was proposed for analyzing the stick-slip and bit bounce using downhole measurements [21]. A major problem with the mechanistic model-based prediction method is that the performance depends strongly on the estimated model parameters. Since model parameters are prone to formation uncertainties, the above methods for calculating model parameters off-line have inherently poor adaptability. Consequently, existing drillstring monitoring methods typically focus on analyzing the fault-sensitive signals or extracting their change features [22].

According to the analysis, there are two major limitations with the methods above: 1) The diagnosis model was developed directly using original drilling signals without considering their physical dependent relationships; 2) Existing static models can hardly meet the safety monitoring demands with the uncertainties of the geological structure, rock type, and drilling mechanical design.

A well-designed monitoring system should be able to detect existing abnormalities as well as achieve early warning of impending faults. According to the discussion, the mechanistic model is helpful in describing variable dependencies from physical kinematics; while the data-driven method becomes powerful as it relies on data to learn the underlying structure of drilling processes. In the era of industrial artificial intelligence, some advanced process monitoring methods incorporate mechanistic knowledge into data-driven models to improve nonstationary process monitoring performance [23, 24]. This provides opportunities to develop a hybrid early warning framework using the drilling data and drillstring mechanism.

Due to formation uncertainty and downhole disturbance, the drillstring exhibits axial and torsional motion in the drilling process. A single-motion model is difficult to describe the motion characteristics of the drillstring accurately. Meanwhile, the drillstring passes through multiple formations in a drilling project. The formation uncertainties, such as the formation trend, rock type, and hardness grade, lead to the normal range of drilling signals being different in various downhole formations. Motivated by the above discussions, this paper proposes an early warning method for drillstring faulty conditions based on multi-model fusion. The contributions are as follows: 1) a hybrid drillstring early warning method is proposed to identify faulty conditions based on the fusion of multi-dimensional prediction models of the drillstring system; 2) an event-triggered model self-updating strategy is proposed to mitigate the prediction performance degradation caused by formation uncertainties.

The rest of the paper is organized as follows: Section 2 describes the problem to be solved. Section 3 presents the systematic method for fault early warning. Section 4 provides the industrial case studies for illustration, followed by discussions and conclusions in Section 5.

2. Problem Description

As shown in Fig. 1, a typical geological drilling system is composed of several components, including a rotary table, draw works, drill line, drillstring, drill bit, and mud pump. The drilling process mainly depends on the drive table rotating the drill bit to break downhole rocks. The rock-breaking power comes from two aspects: 1) the rotary table drives the drill bit to rotate through the drillstring, which transfers the energy from the surface to the drill bit; 2) the draw works controls the pressure applied to the drill bit by changing the speed of the lowering drillstring. Meanwhile, the mud pump pumps the drilling fluid into the wellbore to ensure the borehole stability [3]. The rotational speed of the rotary table is denoted by RPM; the torque of the rotary motor is TRQ; the downward speed of the drillstring is described by Rate Of Penetration (ROP); and the pulling force of the draw works on the drillstring is Hook Load (HKL).

Commonly seen faulty conditions associated with the drillstring include the stuck pipe, bit bounce, washout, and twist-off; these faults account for more than 15% of the non-productive time. The stuck pipe is created from one of several scenarios, such as insufficient hole cleaning and wellbore-geometry issues. The bit bounce is due to the drilling bit being rebounded by the hard downhole formation. The washout is caused by corrosion and abrasion of the drillstring, allowing the drilling fluid to leak into the annulus. If the washout is not detected, it can slowly develop into a twist-off. The above events can be reflected by abnormal changes in measured signals, such as HKL, ROP, TRQ, and RPM. However, sometimes consequent changes in response to the events are minor and not easily captured. Moreover, the drilling mechanism determines that there are strong dependencies between the above four signals. Thus, the original signals, dependencies, and downhole uncertainties should be considered together to detect faulty conditions.

This study aims to design a drillstring safety monitoring method, enabling the early warning of downhole events upon encountering high-risk scenarios, so as to prevent catastrophic accidents. The problem to be solved is to monitor the drilling signals online and capture abnormal changes that are sensitive to faults. First, the prediction models should be developed to describe the normal operating characteristics of the drillstring. Then, the fault early warning can be achieved by comparing the difference between the predicted signal and the online collected signal. Considering the variable geological environments, a model parameter updating strategy is necessary to improve the adaptability of the method.

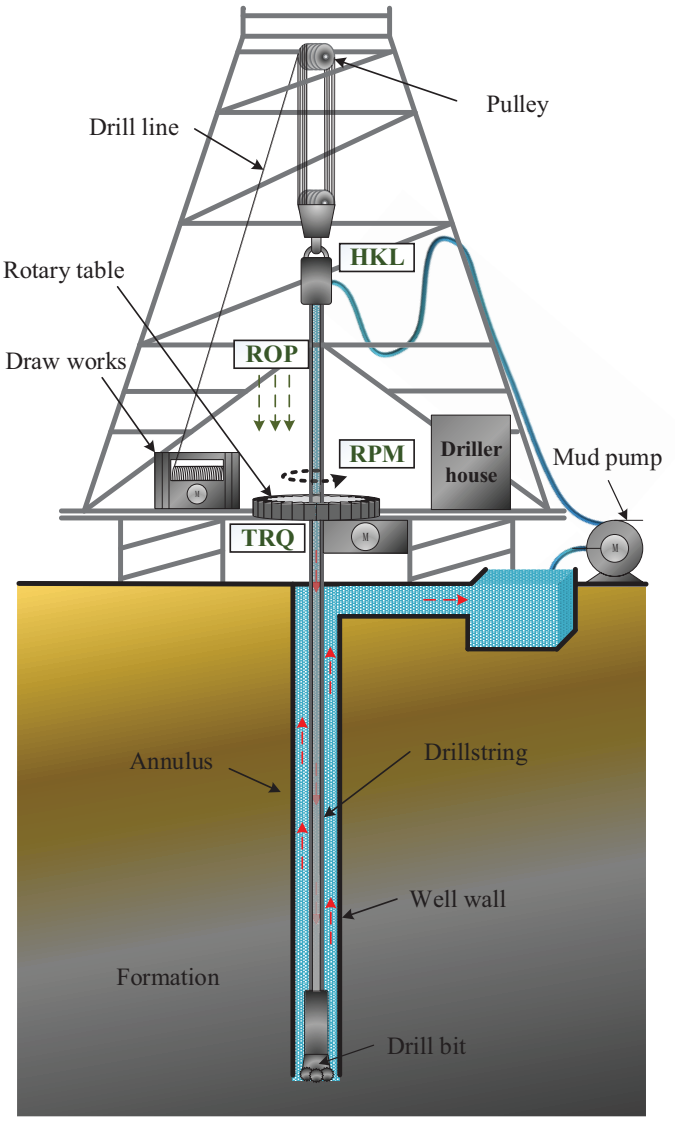

Figure 1: Schematic of a geological drilling process. Key variables associated with drillstring related faults are presented in rectangles. The blue background represents the drilling fluid, and red arrows indicate the flow directions.

3. The proposed fault early warning method

This section presents the drillstring fault early warning method. First, the rotational and axial motion models of the drillstring are developed to predict key variables. Then, residual signals of the key variables are generated and the corresponding alarm thresholds are designed. Next, an event trigger model parameter updating procedure is presented. Last, the early warning scheme is summarized.

3.1. Constructing drillstring motion models

The energy of the drilling process comes from the rotation crush and axial pressure, and the motion characteristics of the drillstring can be described by the rotational and axial motion models.

3.1.1. Rotational motion model

Inspired by rotational motion models for the modeling and control of drillstring [21, 25], a simplified lumped parameter rotational model $\mathcal{M}_r$ without considering the displacements of each drill pipes is given as

$$(J_{rt} + n_0^2 J_m)\ddot{\Theta} + c_v\dot{\Theta} - n_0 T_r = 0, \tag{1}$$

where J_{rt} and J_m denote the inertia of the rotary table and its motor shaft, respectively; T_r represents the Rotary Torque (TRQ); n_0 denotes the motor gearbox ratio of the rotary table; c_v and Θ denote the effective damping and the angular displacement of the drillstring, respectively.

The model in eq. (1) can be rewritten as

$$n_0(J\ddot{\Theta} + c_v\dot{\Theta}) = T_r, \tag{2}$$

where $J = \frac{J_{rt}+n_0^2 J_m}{n_0}$ is the effective inertia. Since the samples are discrete, the discrete form of eq. (2) is expressed as

$$\frac{1}{n_0}\left[J\frac{\big(\dot{\Theta}(k) - \dot{\Theta}(k-1)\big)}{t_s} + c_v\dot{\Theta}(k)\right] = T_r(k), \tag{3}$$

where t_s represents the sample interval, and k denotes the current time stamp. Considering that $\Theta(k)$ cannot be measured directly, the angular velocity is calculated by

$$\dot{\Theta}(k) = \frac{r(k)\pi}{30}, \tag{4}$$

where r denotes the rotational speed of the rotary table (RPM). The relationship between RPM and TRQ is described using the model $\mathcal{M}_r$, which is used to calculate the prediction TRQ signal.

3.1.2. Axial motion model

In the axial direction, the lifting and lowering of the drillstring is controlled by a hosting system. By adjusting the drill line speed via the draw works, the hosting system carries partial gravity of the drillstring with a certain HKL, so as to change the Downhole Weight On Bit (DWOB). Since the DWOB cannot be measured directly, the HKL is used to model the axial motion equation [20]. The axial motion model $\mathcal{M}_a$ of the drillstring is given as [21]

$$m_{\mathrm{ds}}\ddot{x}_{\mathrm{ds}} = m_{\mathrm{ds}}g - F_h, \tag{5}$$

where F_h denotes the hook load, m_{ds} is the suspension mass, and x_{ds} indicates the axial response of the drillstring, which is approximately equal to the hook displacement.

The discrete form of eq. (5) is written as

$$m_{\mathrm{ds}}\frac{\big(v_{\mathrm{ds}}(k) - v_{\mathrm{ds}}(k-1)\big)}{t_s} = \big(m_{\mathrm{ds}}g - F_h(k)\big), \tag{6}$$

$$v_{\mathrm{ds}}(k) = \frac{\big(x_{\mathrm{ds}}(k) - x_{\mathrm{ds}}(k-1)\big)}{t_s}, \tag{7}$$

where v_{ds} denotes the downward speed of drilltsring, which

is equal to ROP, and g indicates the acceleration of gravity.

Considering that the axial response of the drillstring x_{ds} is hard to measure accurately, the draw line displacement x_{dl} is used to calculate it. According to the movable pulley mechanism, the relationship between x_{dl} and x_{ds} is given by

$$x_{\mathrm{ds}}(k) = \mu x_{\mathrm{dl}}(k), \tag{8}$$

where μ is the rope coefficient of the pulley. Based on eqs. (5-8) the relation between HKL, ROP, and axial displacement is established.

3.1.3. Model parameter estimation

After determining the drillstring model structure, another key issue is calculating the model parameters. Some constant values, namely, n_0, t_s, and g can be determined based on the drilling mechanisms. Considering the dynamic and time-varying characteristics of the motion model, parameters such as J and c_v in eq. (3), and m_{ds} in eq. (6) should be estimated using historical drilling data. Either $\mathcal{M}_r$ or $\mathcal{M}_a$ is a single-input single-output discrete model, which can be described as follows

$$\hat{T}_r = \Psi_r(r|J, c_v), \tag{9}$$

$$\hat{F}_h = \Psi_a(x_{\mathrm{ds}}|m_{\mathrm{ds}}), \tag{10}$$

where Ψ_r and Ψ_a denote the functions from r to T_r and x_{ds} to F_h, respectively.

Here, the non-linear least square is used to estimate model parameters, which are determined based on normal historical data [26]. The optimal coefficients in eq. (9) can be obtained by solving

$$\min_{\mathcal{A}} ||\Psi_r(r|\mathcal{A}) - T_r||_2^2 = \min_{\mathcal{A}} \sum_i \left(\Psi_r\left(r(i)|\mathcal{A}\right) - T_r(i)\right)^2, \tag{11}$$

$$\Psi_r(r|\mathcal{A}) = \begin{bmatrix} \Psi_r\left(r(1)|\mathcal{A}\right) \\ \Psi_r\left(r(2)|\mathcal{A}\right) \\ \vdots \\ \Psi_r\left(r(n)|\mathcal{A}\right) \end{bmatrix}. \tag{12}$$

where the set $\mathcal{A} = \{J, c_v\}$. The solution of eq. (11) can be calculated using the Newton method.

3.2. Residual signal generation and alarm threshold design

According to the analysis in Section 2, the drillstring faulty condition can be detected early by monitoring changes in key variables. Here, the first-order residual signal is adopted to describe the changes and generated by calculating the error between the estimated and measured values. On the basis of the established models, $\hat{T}_r$ and $\hat{F}_h$ are estimated online, and then residual signals e_r and e_a of $\mathcal{M}_r$ and $\mathcal{M}_a$ are generated, respectively, as follows:

$$e_r(k) = T_r(k) - \hat{T}_r(k), \tag{13}$$

$$e_a(k) = F_h(k) - \hat{F}_h(k), \tag{14}$$

the values of e_r and e_a are calculated every sample.

To visualize the residual signal characteristics, Fig. 2 shows the histogram plots of e_r and e_a, where the blue and red areas represent the data in normal and faulty conditions, respectively. Designing an alarm threshold that separates normal and abnormal data is difficult due to the overlapping area. Therefore, developing an early warning approach based on amplitude changes is challenging.

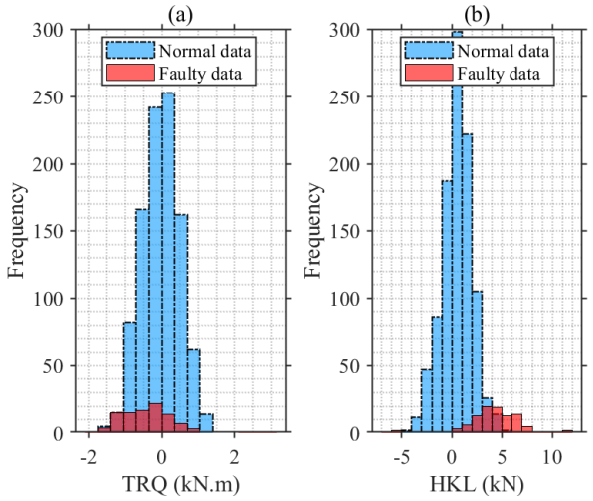

Figure 2: Histograms of residual data of TRQ and HKL in normal and faulty conditions.

Compared to the observation that the residual signals show minor amplitude changes during early faulty states, the residual signal distribution changes significantly during the deterioration from a normal state to a faulty state. From this point of view, the early fault warning can be conducted by detecting changes in the distribution of residual signals. Several metrics to measure the difference between two Probability Density Functions (PDFs) were proposed [27], among which the Wasserstein Distance (WD) method showed good performance by calculating the minimum transfer cost from one PDF to another [28]. For example, the performance of the generated adversarial network is significantly improved by introducing WD to design the loss function. Given two distributions P_1 and P_2 defined on Euclidean space H, the p-Wasserstein distance W_p between P_1 and P_2 is defined by [29]

$$W_p(P_1, P_2) = \left(\inf_{\phi \in \Pi(P_1, P_2)} \int d(\mathbf{x}, \mathbf{y})^p d\phi(\mathbf{x}, \mathbf{y})\right)^{\frac{1}{p}}, \tag{15}$$

where $1 \leq p < \infty$, ϕ indicates a joint probability distribution, $\Pi(P_1, P_2)$ denotes the set of distributions on $H \times H$ with marginal P_1 and P_2, and $d(\mathbf{x}, \mathbf{y})$ is a function of distance cost, where the norm-based cost functions including $||\mathbf{x} - \mathbf{y}||_1$ and $||\mathbf{x} - \mathbf{y}||_2$ are commonly used.

Assume that the sliding window length for the online monitoring is L_1, the residual signals $\mathbf{e}_r(k) = [e_r(k), e_r(k-1), ..., e_r(k - L_1 + 1)]^{\mathrm{T}}$ and $\mathbf{e}(k)_a = [e_a(k), e_a(k -$

$1), ..., e_a(k-L_1+1)]^{\mathrm{T}}$ at $t=k$ compose a residual matrix, i.e., $\mathcal{E} = [\mathbf{e}_r(k), \mathbf{e}_a(k)]$.

The distribution of residual signals can be described using a multivariate Gaussian distribution as

$$p(\mathbf{e}) = \frac{1}{(2\pi)^{\frac{n}{2}}|\Sigma|^{\frac{1}{2}}} \cdot e^{-\frac{1}{2}[(\mathbf{e}-\mu)^{\mathrm{T}}(\Sigma)^{-1}(\mathbf{e}-\mu)]}, \tag{16}$$

where $\mathbf{e} = [e_r, e_a]$, μ is the mean vector, Σ represents the covariance matrix, n denotes the dimension of samples. The μ and Σ can be estimated by

$$\hat{\mu} = \frac{1}{k-L_1+1} \sum_{t=k-L_1+1}^{k} \mathcal{E}_t^{\mathrm{T}}, \tag{17}$$

$$\hat{\Sigma} = \mathbb{E}\Big[(\mathcal{E} - \mathbb{E}[\mathcal{E}])^{\mathrm{T}}(\mathcal{E} - \mathbb{E}[\mathcal{E}])\Big], \tag{18}$$

where the symbol $\mathbb{E}[\cdot]$ represents the expectation function, and $\mathcal{E}_i$ denotes the ith row of $\mathcal{E}$.

The L^2-Wasserstein distance ($p=2$) between $\mathcal{N}_1(\mu_1, \Sigma_1)$ estimated from residual signals under the normal condition and $\mathcal{N}_2(\mu_2, \Sigma_2)$ estimated from $\mathcal{E}$ is given as [29, 28]

$$W_2[\mathcal{N}_1||\mathcal{N}_2] = ||\mu_1-\mu_2||_2^2 + tr\Big[\Sigma_1+\Sigma_2-2(\Sigma_1^{\frac{1}{2}}\Sigma_2\Sigma_1^{\frac{1}{2}})\Big], \tag{19}$$

where $||\mathbf{x}||_2^2 = \mathbf{x}\mathbf{x}^{\mathrm{T}}$, and $tr(\cdot)$ denotes the matrix trace.

To determine whether to generate a fault warning alarm, it just needs to compare the online calculated $W_2(k)$ at $t=k$ with the alarm threshold W_{at},

$$\begin{cases} W_2(k) \le W_{at}: & \text{A normal condition,} \\ W_2(k) > W_{at}: & \text{Fault alarm,} \end{cases} \tag{20}$$

It is worth noting that if the alarm threshold is too low, the normal samples tend to be determined as faults, resulting in massive false alarms. By contrast, higher alarm thresholds may cause the faults to be misclassified as normal conditions, resulting in more missed alarms. Hence, the threshold should be designed based on the statistical characteristics of historical data. Given a confidence level α, the threshold W_{at} is designed to meet the false alarm rate requirement as follows

$$P(w \le W_{at}) = \int_0^{W_{at}} \hat{p}(w)dw = 1-\alpha, \tag{21}$$

where w denotes the random distance variable calculated using eq. (19).

3.3. Event triggered model parameter updating strategy

The hardness and compressive strength of rocks differ in various formations, so the optimal model parameters are different. The prediction model with fixed parameters cannot accurately track changes in drilling signals in complex formations, thus generating false alarms. To overcome formation uncertainties, a model parameter self-updating strategy should be carried out under the fault-free condition if the prediction model shows poor performance in the current formation.

Here, the residual signals e_a and e_r are exploited to determine whether $\mathcal{M}_r$ and $\mathcal{M}_a$ are applicable in the current formation. First, e_a and e_r are segmented by a sliding window of length L_2. Then, the cumulative sum test is introduced to measure the accuracy of the prediction models, where the absolute cumulative modeling errors $S_r(k)$ and $S_a(k)$ are defined as

$$S_r(k) = \left|\sum_{i=1}^{k} e_r(i)\right|, k \le L_2, \tag{22}$$

$$S_a(k) = \left|\sum_{i=1}^{k} e_a(i)\right|, k \le L_2, \tag{23}$$

where k denotes the current time stamp, and $e(k)$ represents the kth sample in the window. As discussed in Section 2, $S_r(k)$ and $S_a(k)$ in the rotational and axial directions should be monitored, respectively. If an error signal changes significantly, the corresponding model parameters must be re-estimated; otherwise, the model parameters remain unchanged. An updating strategy for model parameters is designed by monitoring the cumulative modeling errors, i.e.,

$$A_r(k) = \begin{cases} 0 & \text{if} \quad S_r(k) \le S_r^{th} \\ 1 & \text{otherwise} \end{cases} \tag{24}$$

$$A_a(k) = \begin{cases} 0 & \text{if} \quad S_a(k) \le S_a^{th} \\ 1 & \text{otherwise} \end{cases} \tag{25}$$

where S_r^{th} and S_a^{th} denote the change limits, which are determined based on the historical data using the principle in eq. (21). If $A_r(k)$ or $A_a(k)$ is equal to 1, the corresponding model $\mathcal{M}_r$ or $\mathcal{M}_a$ needs to be updated.

In the field of fault detection in modern industrial systems, the event-triggered mechanism has gained increasing attention [30]. Under the event-triggered framework, an event or alarm is generated only when a predefined triggering condition is satisfied, such that the calculation cost can be reduced. Accordingly, the model parameters are updated in an event-triggered manner based on the cumulative sum test results.

The detailed model parameters updating procedure is summarized in Algorithm 1. Unlike the sliding window L_1 for calculating WD, the L_2 slides window by window rather than sample by sample. The input includes the window length L_2, the residual signals e_r and e_a, the limits S_r^{th} and S_a^{th}, the time stamp t, and k denotes the starting time of the current window. The output includes the model parameters, namely, J, c_v, and m_{ds}.

3.4. Early warning scheme design

The proposed method includes two major phases, namely, fault early warning and parameter self-updating:

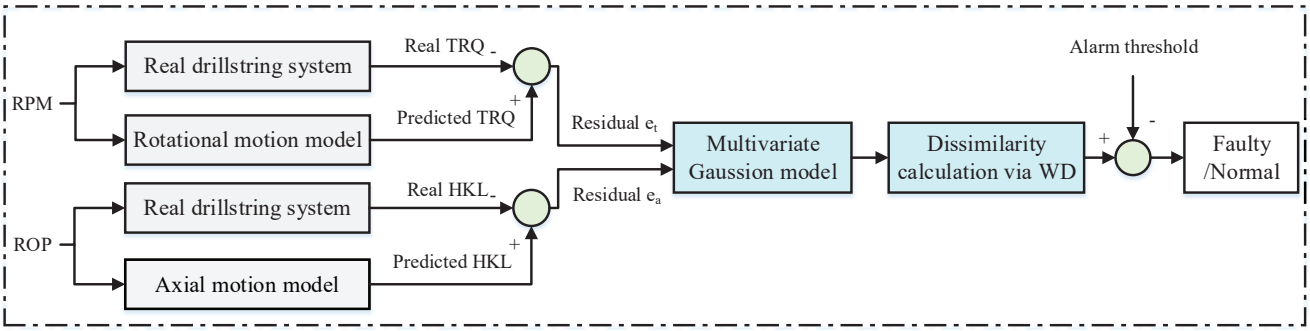

Figure 3: Scheme for the fault early warning phase in the geological drilling process.

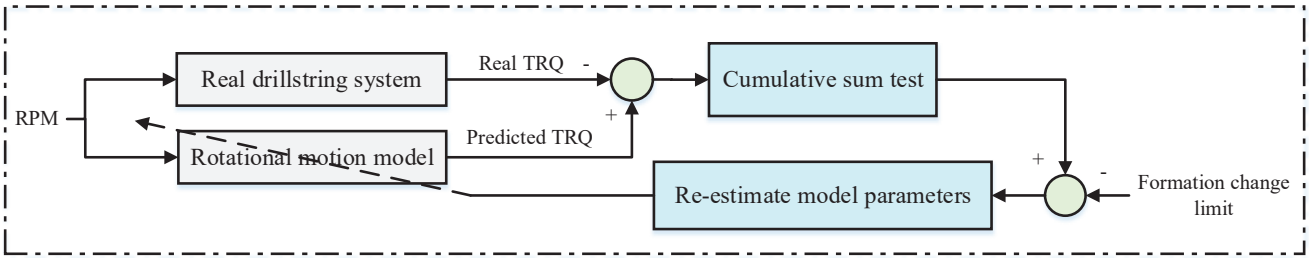

Figure 4: Scheme for the drillstring model parameter self-updating phase, taking the rotational motion model as an example.

Algorithm 1 Event-triggered model parameters updating.

Input Argument: L_2, e_r, e_a, S_r^{th}, S_a^{th}, t, k;
Output Argument: J, c_v, m_{ds};
for $t - k \geq L_2$ **do**
    $k = k + L_2$;
    Slide the window to $[k, k + L_2 - 1]$;
    $S_a = 0$, $S_r = 0$;
end for
if $t - k < L_2$ **then**
    Calculate $S_r(t)$ using eq. (24);
    if $S_r(t) > S_r^{th}$ **then**
        $A_r(t) = 1$;
        Update J and c_v using eq. (11).
    else
        $A_r(t) = 0$;
    end if
    Calculate $S_a(t)$ using eq. (25);
    if $S_a(t) > S_a^{th}$ **then**
        $A_a(t) = 1$;
        Update m_{ds} using eq. (11).
    else
        $A_a(t) = 0$;
    end if
    if $A_r(t) = 1$ or $A_a(t) = 1$ **then**
        $k = t$;
        Slide the window to $[k, k + L_2 - 1]$;
    end if
    $S_a = 0$, $S_r = 0$;
end if

1. Fig. 3 shows the fault early warning phase scheme. First, the rotational and axial motion models of the drillstring are developed based on mechanism structure to predict key variables; Some model parameters are determined based on the drilling rig or technology, while other parameters are estimated based on the non-linear least square using normal historical data. Second, residual signals of the two subsystems are generated based on the predicted and real-time signals. The dissimilarity between the distribution of the online data and that of the normal template data is calculated via WD, so as to obtain the dissimilarity index. Last, the alarm threshold for the dissimilarity index is designed based on normal historical data under a given confidence level; the fault or normal state is determined by comparing the index with the normal threshold.

2. Fig. 4 shows the scheme for the model parameter self-updating phase. If no alarm is generated, the cumulative sum errors for the two prediction models are calculated; the model parameters should be re-estimated if the error exceeds a change limit of the current formation.

To evaluate the fault early warning performance, False Alarm Rate (FAR), Missed Alarm Rate (MAR), and Warning Time (WT) are employed as the criteria. The WT denotes the time interval from the early warning alarm to the occurrence of the fault, and the FAR and MAR are defined as

1) False Alarm Rate

$$P_{\mathrm{FAR}} = \frac{N_{\mathrm{fn}}}{N_{\mathrm{tp}} + N_{\mathrm{fn}}} \times 100\%, \tag{26}$$

2) Missed Alarm Rate

$$P_{\mathrm{MAR}} = \frac{N_{\mathrm{fp}}}{N_{\mathrm{tn}} + N_{\mathrm{fp}}} \times 100\%, \tag{27}$$

where N_{fn} stands for the number of normal samples incorrectly classified into faults, N_{tp} represents the correctly classified normal samples, N_{fp} denotes the normal samples incorrectly classified into faults, and N_{tn} indicates the correctly classified faulty samples.

4. Case study

In this section, drilling data from the ZK3 well were used to demonstrate the effectiveness of the proposed method. The ZK3 well was a geological drilling project located in Hubei Province, China, and the designed depth was 2000 meters. The dataset includes RPM, TRQ, ROP, and HKL; the sampling period was 1 second. The training and validation datasets came from the same well, where normal historical data were used as the training dataset, and the validation dataset included both normal and faulty data. The signal prediction and fault warning performance are demonstrated based on the data collected from the project.

4.1. Signal prediction and fault warning performance

To investigate the effectiveness of the established prediction models, Figs. 5 and 6 show the prediction results of TRQ and HKL under different downhole environments, where the dashed blue curve and solid red curve denote original signals and predicted signals, respectively. In Fig. 5, the predicted signal with the self-updating scheme could track changes in the original signal, especially when there is a significant fluctuation in $t \in [580, 800]$. By contrast, the prediction result with fixed model parameters is shown in Fig. 6, in which a significant deviation existed between the predicted signal and the original signal.

Owing to the changeable formation environment, the prediction performance of a well-trained model with fixed parameters in one formation can be poorer than in another formation. Table 1 summarizes the prediction results of the rotational motion model $\mathcal{M}_r$ and axial motion model $\mathcal{M}_a$, where the fixed parameter and self-updating strategies are used, respectively. The performance is assessed using the Root Mean Squared Error (RMSE) as follow

$$\mathrm{RMSE} = \sqrt{\frac{1}{N}\sum_{j=1}^{N}(x_j - \hat{x}_j)^2}, \tag{28}$$

where N denotes the number of samples, x_j represents the original value, and $\hat{x}_j$ indicates the predicted value. It can

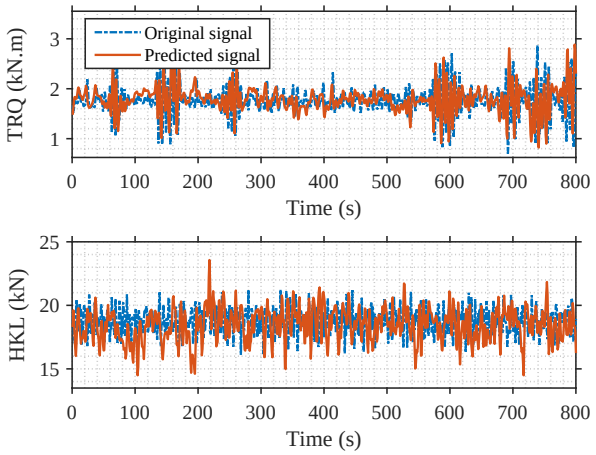

Figure 5: The original and predicted signals of TRQ and HKL, with the self-updating model parameters.

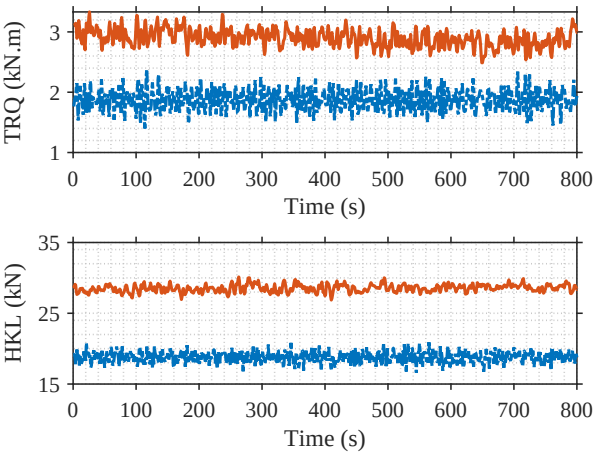

Figure 6: The original and predicted signals of TRQ and HKL, with the fixed model parameters.

Table 1: Comparison of prediction results using different methods with RMSE (%).

	Fixed parameter	Self-updating
$\mathcal{M}_r$	15.11	6.28
$\mathcal{M}_a$	13.39	1.08
Average	14.25	3.68

be found that the result of the self-updating method is significantly better than that of the fixed parameter method. The average RMSE decreased from 14.25% to 3.68%.

To investigate the influence of the sliding window length L_1 on fault early warning performance, Fig. 7 shows the relationship between the Early Warning Time (EWT) and L_1. In general, the shorter L_1 corresponds to the longer ETW. Fig. 8 shows the W distance with different window lengths. In the case of $L_1 = 10$, the W distance signal changes frequently with large amplitude. The W distance signal corresponding to L_1 =250 changes more

slowly, making distinguishing the two upward trends difficult. It indicates that a shorter L_1 is more sensitive to signal changes. However, the short time window can easily lead to false alarms. To balance sensitivity to signal changes with response time to faults, the $L_1 = 60$ was selected for the early warning of drillstring faulty conditions.

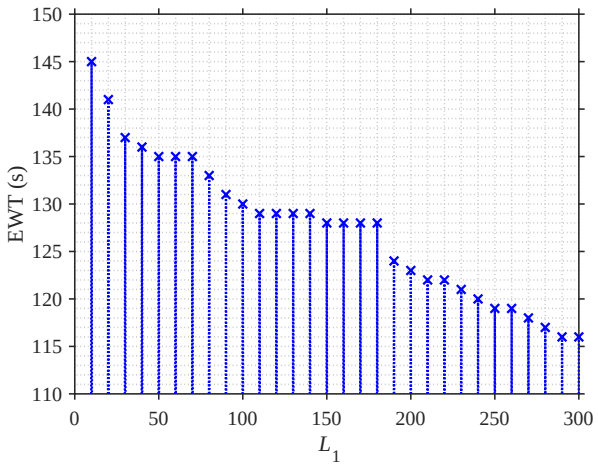

Figure 7: The relationship between the EWT and window length L_1.

4.2. Case 1

This case verifies the superiority of the method for the early warning of a drillstring slip faulty condition. Fig. 9 shows the signal plots and residual generation results. Figs. 9(a) and (b) show the original and predicted signals of TRQ and HKL, respectively. The residual signals e_r and e_a are shown in Figs. 9(c) and (d); the fault early warning results using the Multi-Model based Wasserstein Distance (MM-WD) are presented in Fig. 10, where the blue curve and the red line indicate the W distance and alarm limit, respectively. For comparison, the T^2 and SPE signals based on Principal Component Analysis (PCA) are shown in Fig. 11.

The drillstring was in a normal condition for $t \in [0, 1550]$. Due to changes in the geological structure, the formation cracks encountered by the drill bit caused the drillstring to slide down in $t \in [1550, 1651]$. Then, the signals came back to the normal variation range. At about $t = 1820$, the same event occurred again and lasted longer, reducing the life of the drillstring. As shown in Figs. 9(a)-(d), the differences between the original signal and the predicted signal increased at t=1580, and the differences were more obvious after t=1820. Meanwhile, the W distance signal rose sharply at about $t = 1580$, then peaked at $t = 1810$. The above two increases in the W distance exceeded the normal threshold denoted by the red line, and thus the first short-term faulty symptom and the second continuous fault were both detected. It can be found that the first faulty symptom was detected approximately 200s earlier before the occurrence of the faulty condition, so the fault early warning was achieved.

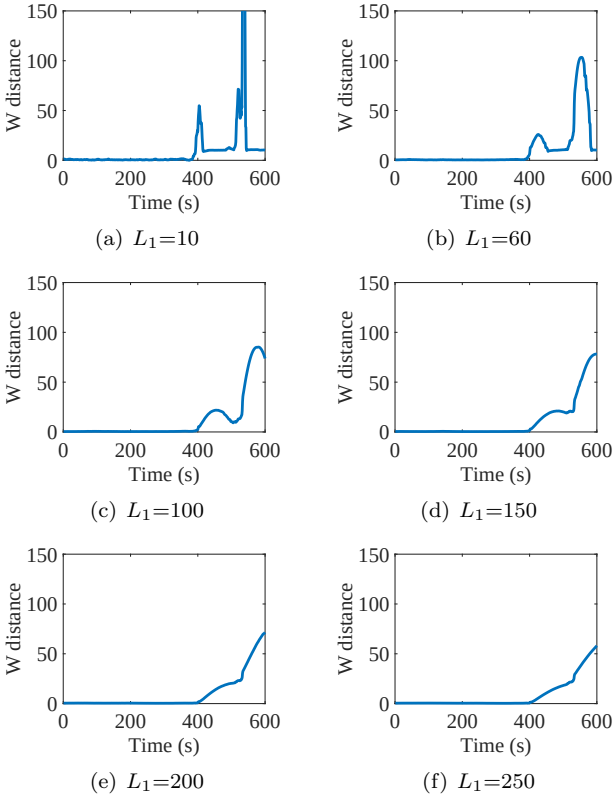

Figure 8: The W distance with different window lengths.

Table 2: Comparison of fault early warning results using different methods in Case 1 (%).

Methods	P_{FAR}	P_{MAR}
T^2	4.30	99.67
SPE	8.63	27.15
AE	7.24	33.44
MM-WD	7.52	7.72

Table 2 presents the fault early warning results using PCA, Autoencoder (AE), and MM-WD methods with respect to the aforementioned drilling process data. The performance of these methods is evaluated by FAR and MAR. The T^2 index has failed to capture the abnormal changes in signals. Although the faulty symptoms were detected by the SPE index, the MAR was higher than 25%. By contrast, the faulty condition was detected using the proposed method with low FAR and MAR, and thus the MM-WD method outperformed the PCA.

4.3. Case 2

This case shows the cycle from normal drilling to abnormal signal changes, and finally to a twist-off fault. Fig. 12 shows the signals during the abnormal condition. The predicted and original signals of HKL and TRQ, and residual signals are shown in Figs. 12(a)-(d). The corresponding W distance signal is shown in Fig. 13.

The drillstring system was in a healthy state before t = 790, and then the drillstring system fell into an abnormal

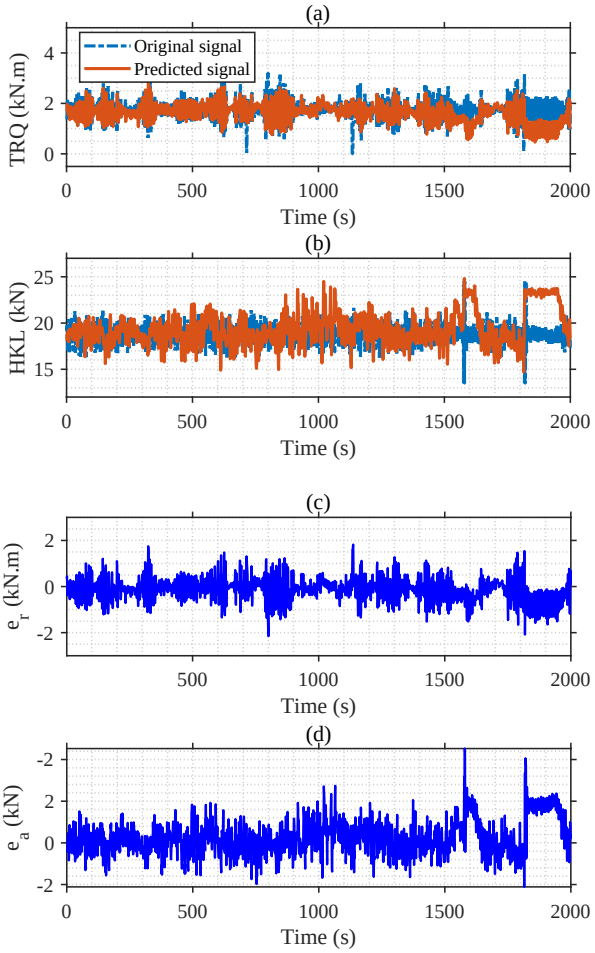

Figure 9: Case 1: (a) and (b) The original and estimated signals of TRQ and HKL; (c) and (d) Time series plots of residual signals e_a and e_r.

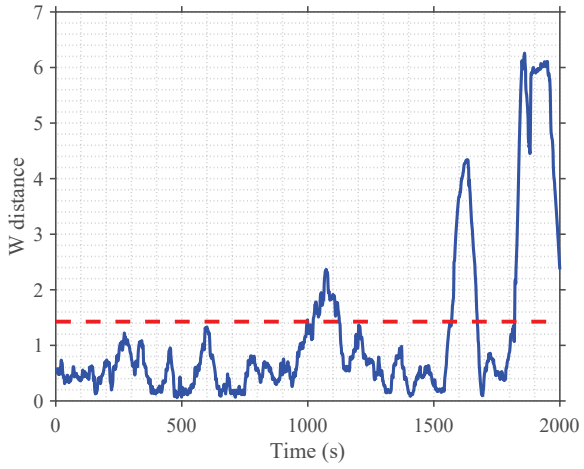

Figure 10: Case 1: W distance using the proposed MM-WD.

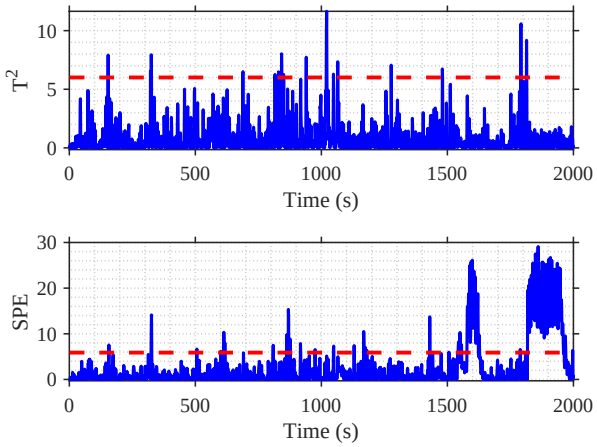

Figure 11: Case 1: Fault warning results using T^2 and SPE.

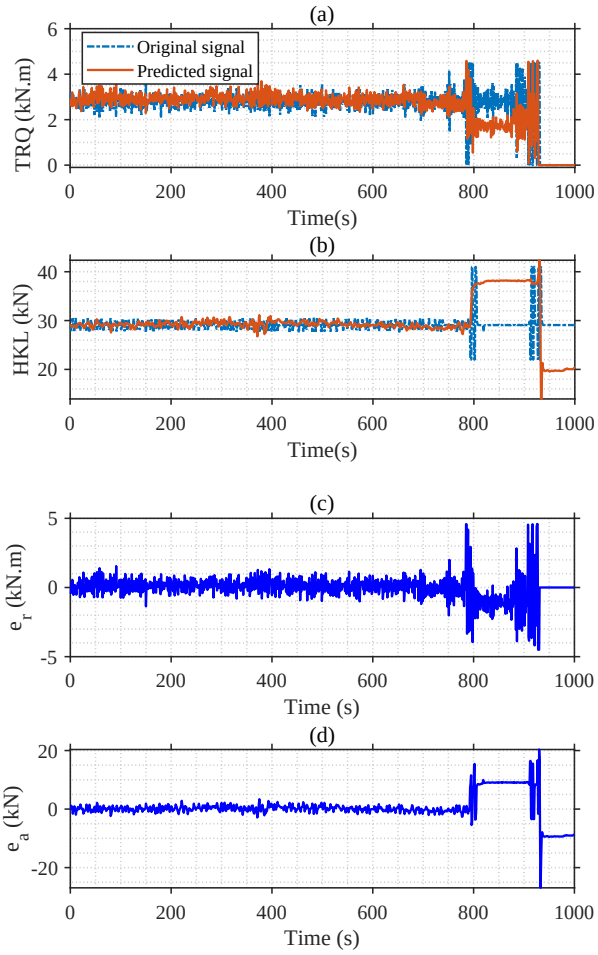

Figure 12: Case 2: (a) and (b) The original and estimated signals of TRQ and HKL; (c) and (d) Time series plots of residual signals e_a and e_r.

condition in $t \in [790, 930]$. After that, the abnormality quickly deteriorated into a twist-off fault. For comparison, the SPE and T^2 signals are shown in Fig. 14.

As shown in Figs. 12(a) and (b), residual signals e_r and e_a climbed at about t=800, and the amplitudes of residual signals increased significantly after t=930. Undesirable

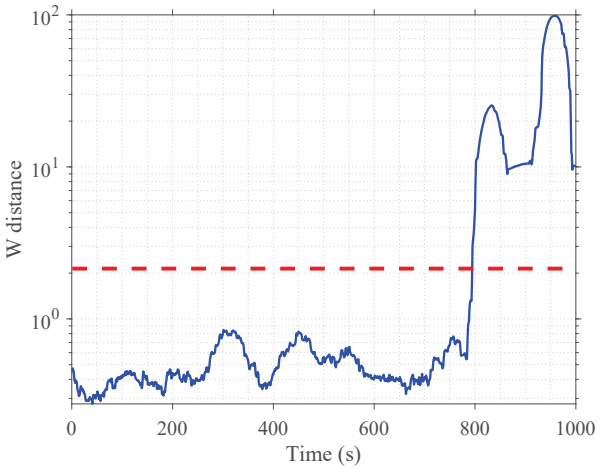

Figure 13: Case 2: W distance using the proposed MM-WD.

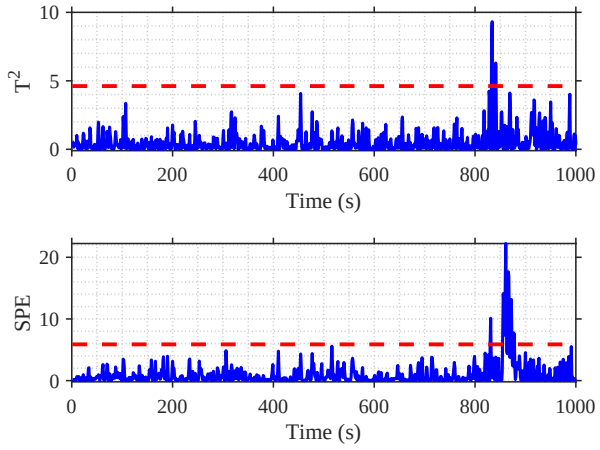

Figure 14: Case 2: Fault warning results using T^2 and SPE.

deviations of e_r and e_a also showed that the system deviated from the normal state. In Fig. 12(e), the W distance signal rose sharply at around t=790, indicating that the abnormality was successfully detected. Next, significant signal changes resulted in a sudden climb of the W distance at around t=900, indicating the deterioration of the fault was also detected. Although the potential abnormality in $t \in [790, 930]$ did not affect normal drilling operations, it was necessary to issue an alarm in advance to avoid the eventual fault. In this way, the fault early warning can be realized. This illustrates that the proposed method can detect abnormal changes before the occurrence of faults and achieve early warning of impending faults.

Table 3 presents the fault early warning results using different methods in Case 2. Although the FARs of T^2 and SPE were acceptable, the MARs of both two methods exceeded 70%. By contrast, the proposed method showed lower FAR and MAR than the PCA-based methods.

Table 3: Comparison of fault early warning results using different methods in Case 2 (%).

Methods	P_{FAR}	P_{MAR}
T^2	8.5	70.67
SPE	1.25	79.33
AE	5.87	50.00
MM-WD	0.75	0.00

5. Conclusion

This paper proposes an original framework for the early warning of drillstring faulty conditions based on multi-model fusion in the complex geological drilling process. First, the rotational and axial drillstring kinematics models were developed to predict fault-sensitive signals. Then, residual signals were generated using the difference between the original signal and the model-predicted signal. After that, the two residual signals were comprehensively described with a multivariate Gaussian distribution. To capture the early signs of faults, the WD was introduced to calculate the difference from the distribution of the online residual signal to that of the reference template. If the difference index violates a predefined threshold, an early fault warning is generated. Furthermore, an event-triggered drillstring model parameters updating procedure is proposed to obtain optimal model parameters in the current formation, so as to overcome the complex and changeable geological environments. Industrial case studies indicate that the proposed method outperforms other approaches. In conclusion, this paper provides a new path to study the drilling fault early warning problem, and the proposed method is expected to help drilling operators detect unexpected downhole events earlier. In future studies, the alarm threshold can be optimized from the perspective of reducing detection delay based on historical fault data.

Declaration of competing interest

The authors declare that they have no known competing financial interests or personal relationships that could have appeared to influence the work reported in this paper.

Acknowledgements

This work was supported by the National Natural Science Foundation of China under Grants 62173313, the 111 project under Grant B17040, and the knowledge Innovation Program of Wuhan-Shuguang Project under Grant 2022010801020208.

References

[1] C. Gan, W.-H. Cao, K.-Z. Liu, M. Wu, A novel dynamic model for the online prediction of rate of penetration and its industrial application to a drilling process, Journal of Process Control 109 (2022) 83–92. doi:https://doi.org/10.1016/j.jprocont.2021.12.002.

[2] M. I. Miah, S. Ahmed, S. Zendehboudi, Model development for shear sonic velocity using geophysical log data: Sensitivity analysis and statistical assessment, Journal of Natural Gas Science and Engineering 88 (2021) 103778. doi:https://doi.org/10.1016/j.jngse.2020.103778.

[3] Y. Li, W. Cao, W. Hu, M. Wu, Detection of downhole incidents for complex geological drilling processes using amplitude change detection and dynamic time warping, Journal of Process Control 102 (2021) 44–53. doi:10.1016/j.jprocont.2021.04.002.

[4] S. J. Hashemi, F. Khan, S. Ahmed, Multivariate probabilistic safety analysis of process facilities using the copula bayesian network model, Computers & Chemical Engineering 93 (2016) 128–142. doi:https://doi.org/10.1016/j.compchemeng.2016.06.011.

[5] Z. Wu, D. Rincon, P. D. Christofides, Process structure-based recurrent neural network modeling for model predictive control of nonlinear processes, Journal of Process Control 89 (2020) 74–84. doi:https://doi.org/10.1016/j.jprocont.2020.03.013.

[6] W. Yu, C. Zhao, B. Huang, Recursive cointegration analytics for adaptive monitoring of nonstationary industrial processes with both static and dynamic variations, Journal of Process Control 92 (2020) 319–332. doi:https://doi.org/10.1016/j.jprocont.2020.06.013.

[7] C. Shang, B. Huang, F. Yang, D. Huang, Slow feature analysis for monitoring and diagnosis of control performance, Journal of Process Control 39 (2016) 21–34. doi:https://doi.org/10.1016/j.jprocont.2015.12.004.

[8] A. U. Osarogiagbon, F. Khan, R. Venkatesan, P. Gillard, Review and analysis of supervised machine learning algorithms for hazardous events in drilling operations, Process Safety and Environmental Protection 147 (2021) 367–384. doi:10.1016/j.psep.2020.09.038.

[9] A. K. Abbas, A. A. Bashikh, H. Abbas, H. Q. Mohammed, Intelligent decisions to stop or mitigate lost circulation based on machine learning, Energy 183 (2019) 1104–1113. doi:10.1016/j.energy.2019.07.020.

[10] N. Tsuchihashi, R. Wada, M. Ozaki, T. Inoue, K. R. Mopuri, H. Bilen, T. Nishiyama, K. Fujita, K. Kusanagi, Early stuck pipe sign detection with depth-domain 3D convolutional neural network using actual drilling data, SPE Journal 26 (02) (2021) 551–562. doi:10.2118/204462-PA.

[11] Y. Li, W. Cao, W. Hu, M. Wu, Diagnosis of downhole incidents for geological drilling processes using multi-time scale feature extraction and probabilistic neural networks, Process Safety and Environmental Protection 137 (2020) 106–115. doi:10.1016/j.psep.2020.02.014.

[12] Z. Zhang, X. Lai, M. Wu, L. Chen, C. Lu, S. Du, Fault diagnosis based on feature clustering of time series data for loss and kick of drilling process, Journal of Process Control 102 (2021) 24–33. doi:10.1016/j.jprocont.2021.03.004.

[13] Y. Li, W. Cao, W. Hu, M. Wu, Abnormality detection for drilling processes based on Jensen-Shannon divergence and adaptive alarm limits, IEEE Transactions on Industrial Informatics 17 (9) (2021) 6104–6113. doi:10.1109/TII.2020.3032433.

[14] O. S. Ahmed, B. M. Aman, M. A. Zahrani, F. I. Ajikobi, Stuck pipe early warning system utilizing moving window machine learning approach, in: Abu Dhabi International Petroleum Exhibition and Conference, 2019. doi:10.2118/197674-MS.

[15] Y. Li, W. Cao, W. Hu, Y. Xiong, M. Wu, Incipient fault detection for geological drilling processes using multivariate generalized gaussian distributions and Kullback-Leibler divergence, Control Engineering Practice 117 (2021) 104937. doi:https://doi.org/10.1016/j.conengprac.2021.104937.

[16] Z. Yu, Y. Zhang, B. Jiang, C.-Y. Su, J. Fu, Y. Jin, T. Chai, Fractional order PID-based adaptive fault-tolerant cooperative control of networked unmanned aerial vehicles against actuator faults and wind effects with hardware-in-the-loop experimental validation, Control Engineering Practice 114 (2021) 104861. doi:https://doi.org/10.1016/j.conengprac.2021.104861.

[17] A. Willersrud, M. Blanke, L. Imsland, A. Pavlov, Fault diagnosis of downhole drilling incidents using adaptive observers and statistical change detection, Journal of Process Control 30 (2015) 90–103. doi:10.1016/j.jprocont.2014.12.010.

[18] H. Jiang, G. Liu, J. Li, T. Zhang, C. Wang, K. Ren, Model based fault diagnosis for drillstring washout using iterated unscented kalman filter, Journal of Petroleum Science and Engineering 180 (2019) 246–256. doi:10.1016/j.petrol.2019.05.043.

[19] T. Vromen, C. Dai, N. van de Wouw, T. Oomen, P. Astrid, A. Doris, H. Nijmeijer, Mitigation of torsional vibrations in drilling systems: A robust control approach, IEEE Transactions on Control Systems Technology 27 (1) (2019) 249–265. doi:10.1109/TCST.2017.2762645.

[20] S. Ma, M. Wu, L. Chen, C. Lu, W. Cao, Robust mixed-sensitivity H_∞ control of weight on bit in geological drilling process with parameter uncertainty, Journal of the Franklin Institute 358 (13) (2021) 6433–6461. doi:10.1016/j.jfranklin.2021.06.005.

[21] J. M. Kamel, A. S. Yigit, Modeling and analysis of stick-slip and bit bounce in oil well drillstrings equipped with drag bits, Journal of Sound and Vibration 333 (25) (2014) 6885–6899. doi:10.1016/j.jsv.2014.08.001.

[22] A. D. Paul, B. M. N., Early detection of drillstring washouts based on downhole turbine RPM monitoring prevents twist-offs in challenging drilling environment in india, in: IADC/SPE Asia Pacific Drilling Technology Conference and Exhibition, 2008. doi:10.2118/197674-MS.

[23] X. Chen, C. Zhao, Conditional discriminative autoencoder and condition-driven immediate representation of soft transition for monitoring complex nonstationary processes, Control Engineering Practice 122 (2022) 105090. doi:https://doi.org/10.1016/j.conengprac.2022.105090.

[24] C. Zhao, Perspectives on nonstationary process monitoring in the era of industrial artificial intelligence, Journal of Process Control 116 (2022) 255–272. doi:https://doi.org/10.1016/j.jprocont.2022.06.011.

[25] M. V. Faronov, I. G. Polushin, Observer-based control of vertical penetration rate in rotary drilling systems, Journal of Process Control 106 (2021) 29–43. doi:https://doi.org/10.1016/j.jprocont.2021.08.016.

[26] Y. Si, Y. Wang, D. Zhou, Key-performance-indicator-related process monitoring based on improved kernel partial least squares, IEEE Transactions on Industrial Electronics 68 (3) (2021) 2626–2636. doi:10.1109/TIE.2020.2972472.

[27] H. Chen, B. Jiang, S. X. Ding, N. Lu, W. Chen, Probability-relevant incipient fault detection and diagnosis methodology with applications to electric drive systems, IEEE Transactions on Control Systems Technology 27 (6) (2019) 2766–2773. doi:10.1109/TCST.2018.2866976.

[28] Y. Chen, J. Ye, J. Li, Aggregated wasserstein distance and state registration for hidden markov models, IEEE Transactions on Pattern Analysis and Machine Intelligence 42 (9) (2020) 2133–2147. doi:10.1109/TPAMI.2019.2908635.

[29] C. R. Givens, R. M. Shortt, A class of Wasserstein metrics for probability distributions, Michigan Mathematical Journal 31 (2) (1984) 231–240. doi:10.1307/mmj/1029003026.

[30] X. Wang, Z. Fei, H. Yan, Y. Xu, Dynamic event-triggered fault detection via zonotopic residual evaluation and its application to vehicle lateral dynamics, IEEE Transactions on Industrial Informatics 16 (11) (2020) 6952–6961. doi:10.1109/TII.2020.2972033.